Fast ion power loads on ITER first wall structures in the presence of NTMs and microturbulence

IOP Publishing and International Atomic Energy Agency Nuclear Fusion
Nucl. Fusion **51** (2011) 083041 (10pp) doi:10.1088/0029-5515/51/8/083041

Fast ion power loads on ITER first wall structures in the presence of NTMs and microturbulence

T. Kurki-Suonio[1], O. Asunta[1], E. Hirvijoki[1], T. Koskela[1], A. Snicker[1], T. Hauff[2], F. Jenko[2], E. Poli[2] and S. Sipilä[1]

[1] Aalto University, Assn Euratom-Tekes, PO Box 14100, FI-00076 AALTO, Finland
[2] Max-Planck-Institut für Plasmaphysik, EURATOM Association, Boltzmannstrasse 2, D-85748 Garching, Germany

Received 30 December 2010, accepted for publication 1 July 2011
Published 28 July 2011
Online at stacks.iop.org/NF/51/083041

Abstract
The level and distribution of the wall power flux of energetic ions in ITER have to be known accurately in order to ensure the integrity of the first wall. Until now, most quantitative estimates have been based on the assumption that fast ion transport is dictated by neoclassical effects only. However, in ITER, the fast ion distribution is likely to be affected by various MHD effects and probably also by microturbulence. We have now upgraded our orbit-following Monte Carlo code ASCOT so that it has simple, theory-based models for neoclassical tearing mode (NTM)-type islands as well as for turbulent diffusion. ASCOT also allows for full-orbit following, which is important close to the material surfaces and, possibly, also when strong toroidal inhomogeneities are present in the magnetic field. Here we introduce the new models, preliminary results obtained with them, and how these models could be made more realistic in the future. The simulations are carried out for thermonuclear alpha particles in ITER scenario 2 plasma, because we consider this combination to be most critical for the successful operation of ITER. Neither the turbulent transport nor NTM-type islands are found to introduce alarming changes in the wall loads. However, at this stage it was not possible to combine the island structures with the non-axisymmetric magnetic field of ITER, and it remains to be seen what the combined effect of drift islands together with the toroidal ripple and local field aberrations, such as those due to test blanket modules and resonant magnetic perturbations will be.

(Some figures in this article are in colour only in the electronic version)

1. Introduction

The new physics introduced by ITER operation is related to the very energetic (3.5 MeV) alpha particles produced in large quantities in fusion reactions. These particles not only constitute a massive energy source inside the plasma but also present a potential hazard to the material structures that provide the containment of the burning plasma. In addition, the negative neutral beam injection produces 1 MeV deuterons, and the application of ICRH creates minority ions in the multi-MeV range [1].

The finite number (18 in ITER) and limited toroidal extent of the toroidal field (TF) coils cause a periodic variation of the TF called the magnetic ripple. This ripple can provide a significant channel for fast particle leakage, leading to very localized fast particle loads on the walls. Because the ripple could cause significant additional ion transport [2, 3], ferromagnetic inserts (FIs) will be embedded in the double wall structure of the ITER vacuum vessel in order to reduce the ripple [1, 4]. In ITER, the TF deviations are locally further enhanced by the presence of discrete ferromagnetic structures such as the test blanket modules (TBMs) [5] that cause poloidally and toroidally localized perturbations to the magnetic field [6, 7]. We shall refer to this local perturbation as 'TBM field bump' to distinguish it from the global toroidal ripple exhibiting the 18-fold symmetry of the TF coils.

We have previously carried out a preliminary study of the wall loads caused by three types of fast particles; fusion-born alpha particles, deuterons from neutral beam injection (NBI), and ICRH-heated minority ions, in a variety of ITER plasmas using the 5D Monte Carlo guiding-centre code (GC) ASCOT [8]. The simulations were performed for different magnetic field configurations, including FIs and none or more TBMs. These simulations were carried out using input data that has later been either changed (the wall structure and geometry of the FIs) or found deficient (the 3D magnetic background corresponding to the situation with TBMs).

Furthermore, all simulations thus far have been based on the assumption that the fast ion transport is dominated by neoclassical effects. In MHD quiescent plasmas this

was believed to be true until the first NBI current drive experiments with the ASDEX Upgrade tangential beams failed to demonstrate the predicted levels of off-axis current [9] except at very low NBI power. Subsequent theoretical work has revealed that, contrary to what was previously believed, microturbulence can induce additional transport of not just the bulk plasma but also the fast ions [10]. Furthermore, it is highly unlikely that ITER plasmas will be MHD quiescent: the massive fast ion population consisting of fusion alphas with energies up to 3.5 MeV drive a multitude of Alfvénic modes and other energetic particle modes, which in turn act back on the fast ion population [11]. Furthermore, ITER is prone to neoclassical tearing modes (NTMs) with substantial island structures [12]. All of these MHD phenomena can contribute to increased transport of fast ions in the core plasma [13]. This in turn increases the fast ion population at the edge where the transport due to field aberrations caused by the TF coils and TBMs can lead to unacceptably high peak power loads on some first wall components. None of the GC codes presently in use worldwide can account for all of these effects.

We have begun incorporating effects of plasma instabilities on fast ion transport into ASCOT. It now has a theory-based model for anomalous diffusion due to microturbulence [10] and a model of magnetic islands due to NTMs [14, 15]. Furthermore, concerns have been expressed that in the presence of significant toroidal inhomogeneities in the magnetic field, the GC approach would not be sufficient. To resolve this issue we have now refurbished ASCOT with the option to follow the full Larmor orbits [16]. Since full-orbit (FO) following is very time consuming, ASCOT also provides an option to switch between GC and FO following in the vicinity of the wall.

In this paper we present the first simulation results of fusion alpha power loads on ITER plasma-facing components (PFCs) taking into account the fast ion redistribution due to microturbulence and NTMs. The simulations are carried out with the most recent 3D wall design [17], but the results are also compared with power loads obtained assuming axisymmetric wall and with loads on the older, 2-limiter wall configuration. We also investigate the redistribution of fast ions in the core plasma due to these physical mechanisms. The simulations should be carried out for two different ITER plasmas: scenario 2, which is a standard H-mode, and scenario 4, which corresponds to steady-state operation. In the earlier, neoclassical study, the wall power loads were found insignificant in scenario 4 and much larger but still easily tolerable even in scenario 2. The difference arises from the different plasma profiles: in scenario 4, temperature and density profiles are much steeper, which causes thermal fusions and ionization of NBI particles to occur only close to the plasma core. Therefore it is expected that the redistribution of fast ions due to non-neoclassical effects can be particularly treacherous in scenario 4: drift islands and anomalous transport lead energetic ions to the edge where additional transport processes induced by 3D field aberrations rapidly take them to the first wall components. However, here we shall focus only on fusion alphas in scenario 2 for the following reasons: (i) we consider scenario 2 more critical because it will be the one adopted before the more advanced scenario 4 and its fusion power is significantly higher (500 MW versus 360 MW); (ii) including also thermal load on the wall, scenario 2 is likely to have higher total power fluxes to the PFCs than scenario 4; (iii) in the earlier study [8], the fast ions produced by external heating were not found important in scenario 2, thus only alphas are simulated; (iv) scenario 2 has a q profile that enables (2,1) and (3,2) NTMs to exist.

The structure of the paper is as follows: in section 2 we introduce the island model adopted in ASCOT, while in section 3 the turbulent transport model is described. Section 4 presents the simulation results including the new physics. There we also briefly describe the 3D ITER wall structures, both the old version with only two limiters and the new 'continuous limiter' version. The paper is concluded and future prospects are discussed in section 5.

2. Numerical model for islands in ASCOT

The most obvious way to implement islands would be to add them as perturbations to magnetic background data. However, reconstructing a discrete 3D magnetic background with a host of field aberrations, including islands, for fast ion simulations is a non-trivial task. Between collisions the fast ions complete hundreds of orbits and, consequently, any error in their orbit due to inaccuracies in the magnetic field will be amplified, leading to numerical drifts. This problem can be somewhat alleviated using acceleration of the interaction time scales [8], but this method also becomes of limited use with increasing complexity of the field. This issue with discrete magnetic backgrounds was first raised in the context of TBM field bumps [8], and later concerns were voiced that reliable fast ion simulations would actually require a 3D equilibrium reconstruction. The latter issue was carefully investigated [18], and it was concluded that, fortunately, the more traditional tokamak approach of combining a 2D equilibrium with a vacuum field with 3D features is sufficient.

Since the integrity of the magnetic background is of such importance, we decided not to incorporate the island structures directly into the components of the magnetic background field but, instead, adopted another approach [14]. We use a relativistic Hamiltonian formalism in deriving the equation of motion in magnetic coordinates and add the effect of magnetic islands as a perturbation in the magnetic vector potential as in [14]. The perturbation describing NTMs is given by [19]

$$\tilde{\boldsymbol{A}}_{\mathrm{NTM}} = \sum_{n,m} A_{m,n}(\psi)\cos(m\theta - n\zeta)\,\boldsymbol{B}, \tag{1}$$

where the amplitudes $A_{m,n}$ for the different modes can be functions of the poloidal flux ψ used as a radial coordinate. Here, m is the poloidal mode number and n is the toroidal mode number, while θ and ζ are angles of the Boozer–White coordinate system, as defined in [20]. For the radial profile $A_{m,n}$ we use a theory-based parametrization [21] describing resistive modes

$$A_{m,n}(\psi) = \rho_{m,n}\alpha\left(\frac{\psi}{\psi_{m,n}}\right)^{m/2}\left(1-\beta\left(\frac{\psi}{\psi_{m,n}}\right)^{1/2}\right),$$
$$\text{for } \psi \leqslant \psi_{m,n},$$
$$A_{m,n}(\psi) = \rho_{m,n}\frac{\alpha(1-\beta)-\gamma+\gamma\left(\frac{\psi}{\psi_{m,n}}\right)^{1/2}}{(\psi/\psi_{m,n})^{(m+1)/2}},$$
$$\text{for } \psi > \psi_{m,n}. \tag{2}$$

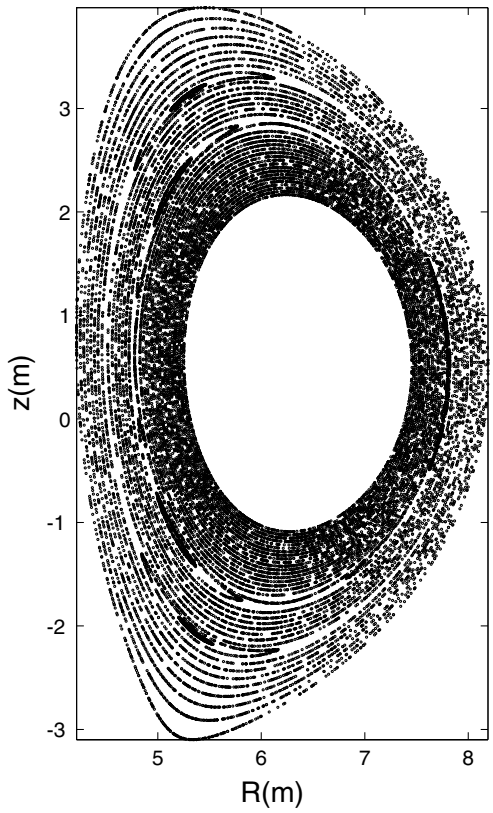

Figure 1. A Poincaré plot of the (3,2) and (2,1) perturbations used in this work. The background magnetic field corresponds to the ITER scenario 2 operation.

where $\psi_{m,n}$ is the poloidal flux corresponding to the resonance surface with $q = m/n$. For the time being, we are limited to modes inside the separatrix, i.e. $A_{m,n} = 0$ outside the last closed flux surface. The values for the parameters $\rho_{m,n}$, α, β and γ are chosen so that the island width, the island position and the radial perturbation field strength correspond to experimental measurements (from electron cyclotron emission, soft x-ray signal and Mirnov coils, respectively) in present-day tokamaks or, in the case of ITER, to numerical estimates.

The model has already been used in ASDEX Upgrade [19] to analyse fast ion losses due to NTMs. There, measured values for island parameters were used, and the results were compared against measured fast ion losses. Preliminary ASCOT results on fast ion confinement using this model were reported in EPS 2010 [22]. In this paper, a numerical estimate for the island width is taken from [23] while other parameters are obtained from [19]. Aside from the island width, varying the other parameters by up to an order of magnitude did not appear to dramatically change the island structure. Figure 1 shows the island structures used in this work.

3. Numerical model for turbulent diffusion of fast ions in ASCOT

Until now, ASCOT, like most other GC codes attempting to include anomalous effects, has used diffusion coefficients D that are either constant or exhibit some radial and/or energy dependence that is included on an ad hoc basis. Recently, a theory-based model for the fast ion diffusion coefficient has been published [10], deriving the value of the diffusion coefficient from the properties of the plasma background and the resulting microturbulence. Both electrostatic and magnetic turbulence were addressed, and the corresponding diffusion coefficients, D_E and D_B, were calculated separately for strongly trapped and strongly passing particles. According to the model, the effect of turbulence does not fall off with energy as rapidly as previously thought. Instead, in the case of electrostatic turbulence, the anomalous diffusion falls off only as $E^{-0.5...-1.0}$ ($E^{-0.5}$ for small and $E^{-1.0}$ for large pitch angles), and in the case of magnetic turbulence as $E^{-0.5...0.0}$. The diffusion is expected to be radial because the turbulent structures vary more strongly in the perpendicular than in the parallel direction. We have now implemented this numerical diffusion model into ASCOT in order to get more realistic values, not only for the peak power loads on ITER walls but for the neutral beam driven current as well.

The traditional way of incorporating non-neoclassical transport effects into GC simulations is based on the work by Boozer and Kuo-Petravic [24]. Starting from the diffusion equation

$$\frac{\partial f}{\partial t} = \nabla \cdot (D \nabla f), \tag{3}$$

one can derive the corresponding radial diffusion equation:

$$\frac{\partial f}{\partial t} = \frac{1}{s(\psi)} \frac{\partial}{\partial \psi} \left[s |\nabla \psi|^2 D \frac{\partial f}{\partial \psi} \right]. \tag{4}$$

Here ψ is the poloidal magnetic flux, and the flux surface area $s(\psi)$, introduced by the divergence operator in equation 3, is defined so that the volume element of physical space is $\mathrm{d}^3x = s(\psi)\mathrm{d}\psi$. (Adding in the multiplier $|\nabla\psi|^2$ allows the diffusion coefficient D to be given in its natural units, $[D] = \mathrm{m}^2\mathrm{s}^{-1}$.) Using binomial statistics, it is possible to derive the corresponding Monte Carlo operator:

$$\begin{aligned} \Delta\psi &= \frac{\mathrm{d}}{\mathrm{d}t} \langle\psi\rangle \, \Delta t + \delta \sqrt{\frac{\mathrm{d}}{\mathrm{d}t} \left(\langle\psi^2\rangle - \langle\psi\rangle^2 \right) \Delta t} \\ &= \frac{1}{s} \frac{\partial}{\partial \psi} \left(s |\nabla\psi|^2 D \right) \Delta t + \delta \sqrt{2 |\nabla\psi|^2 D \Delta t}, \end{aligned} \tag{5}$$

where the first deterministic term gives the mean drift. The second stochastic term, where $\delta = \pm 1$ is a random sign, generates the desired standard deviation to the distribution. The deterministic term seems to be typically at least an order of magnitude smaller than the stochastic term, but because of its cumulative nature it can still play an important role in longer simulations. When calculating the expectation values, the distribution function of the test particle is taken to be a δ-function in ψ.

In ASCOT, the ρ_{pol} is used as a radial coordinate. From here on, it is simply called ρ, and defined as $\rho = \sqrt{(\psi - \psi_{\mathrm{axis}})/(\psi_{\mathrm{sep}} - \psi_{\mathrm{axis}})}$. After every time step Δt, the diffusion operator moves the particle perpendicular to the flux surfaces over distance $\Delta\rho$. Since the fundamental mechanism by which the diffusion occurs is the $\boldsymbol{E} \times \boldsymbol{B}$ drift, energy should be (approximately) conserved over this displacement, leaving one degree of freedom in how it is distributed among $v_\parallel$ and $v_\perp$. Currently the operator keeps both velocity components constant. Consequently, the magnetic moment μ of the particle is changed.

Initially, Hauff *et al* derived the model only for strongly passing and strongly trapped particles [10]. For ASCOT simulations, however, valid expressions for the diffusion coefficients are needed for all orbit topologies. In [25], the diffusion coefficients published in [10] have been extended to arbitrary values of the particle pitch $\xi \equiv v_\parallel/v$ and to both large and small gyroradii. In addition to the pitch dependence, the diffusion coefficients explicitly depend on the energy of the particle. The microturbulence enters the diffusion coefficients in the form of correlation lengths and, in the case of electrostatic turbulence, the $\boldsymbol{E}\times\boldsymbol{B}$ velocity. The plasma background, in the form of local temperature values, also enters the equations for the diffusion coefficients. We now proceed to present the equations for diffusion coefficients due to electrostatic and magnetic microturbulence as they are given in [25] and used in ASCOT.

For passing particles with a small gyroradius, $(E/\hat{\lambda}_c T_i)(1-\xi_{max}^2) < 0.132$:

$$D_E = \frac{\hat{V}_E^2\hat{\lambda}_V}{3\xi_{max}^2}\left(\frac{E}{T_e}\right)^{-1}\left[1-\frac{5}{2\hat{\lambda}_c^2}\frac{E}{T_e}(1-\xi_{max}^2)\right]\frac{\rho_i^2 c_i}{R_0}, \quad (6)$$

and

$$D_B = \frac{(C\beta/\beta_{crit})^2\hat{\lambda}_B}{3}\left[1-\frac{5}{2\hat{\lambda}_c^2}\frac{E}{T_e}(1-\xi_{max}^2)\right]\frac{\rho_i^2 c_i}{R_0}. \quad (7)$$

For trapped particles with a small gyroradius:

$$D_E = \frac{2\hat{V}_E^2\hat{\lambda}_c\sqrt{\epsilon}}{3\sqrt{\xi_{max}^2(1-\xi_{max}^2)}}\left(\frac{E}{T_e}\right)^{-1} \times\left[1-\frac{5}{2\hat{\lambda}_c^2}\frac{E}{T_e}(1-\xi_{max}^2)\right]\frac{\rho_i^2 c_i}{R_0}, \quad (8)$$

and

$$D_B = \frac{2(C\beta/\beta_{crit})^2\hat{\lambda}_B\sqrt{\epsilon}|\xi_{max}|}{3\sqrt{1-\xi_{max}^2}} \times\left[1-\frac{5}{2\hat{\lambda}_c^2}\frac{E}{T_e}(1-\xi_{max}^2)\right]\frac{\rho_i^2 c_i}{R_0}. \quad (9)$$

For passing particles with a large gyroradius, $(E/\hat{\lambda}_c T_i)(1-\xi_{max}^2) > 0.132$:

$$D_E = \frac{1.73\hat{V}_E^2\hat{\lambda}_c\hat{\lambda}_V}{12\sqrt{\pi(1-\xi_{max}^2)}\xi_{max}^2}\left(\frac{E}{T_e}\right)^{-3/2}\frac{\rho_i^2 c_i}{R_0} \quad (10)$$

and

$$D_B = \frac{1.73(C\beta/\beta_{crit})^2\hat{\lambda}_B^2}{12\sqrt{\pi(1-\xi_{max}^2)}}\left(\frac{E}{T_e}\right)^{-1/2}\frac{\rho_i^2 c_i}{R_0}. \quad (11)$$

For trapped particles with a large gyroradius:

$$D_E = \frac{1.73\hat{V}_E^2\hat{\lambda}_c\hat{\lambda}_V\sqrt{\epsilon}}{12\sqrt{\pi}|\xi_{max}|(1-\xi_{max}^2)}\left(\frac{E}{T_e}\right)^{-3/2}\frac{\rho_i^2 c_i}{R_0} \quad (12)$$

and

$$D_B = \frac{1.73(C\beta/\beta_{crit})^2\hat{\lambda}_B^2\sqrt{\epsilon}|\xi_{max}|}{12\sqrt{\pi}(1-\xi_{max}^2)}\left(\frac{E}{T_e}\right)^{-1/2}\frac{\rho_i^2 c_i}{R_0}. \quad (13)$$

In these equations, T_e stands for the local electron temperature, and ρ_i and c_i are the thermal ion Larmor radius and sound speed, respectively. The radial dependence is manifested through these local parameters. In equations (6)–(13), the turbulence is characterized by the mean magnitude of the radial component of the $\boldsymbol{E}\times\boldsymbol{B}$ drift ($\hat{V}_E$), as well as the normalized electrostatic potential and the $\boldsymbol{E}\times\boldsymbol{B}$ correlation lengths ($\hat{\lambda}_c$ and $\hat{\lambda}_V$, respectively). Their values should be determined from experiment or from turbulence simulations. The radial correlation lengths have been experimentally measured to be in the range 5–10 ρ_s [26], while simulations of ITG and TEM turbulence have yielded the value $\lambda_c \sim 6\rho_s$. For the $\boldsymbol{E}\times\boldsymbol{B}$ drift we use the estimate $\hat{V}_E = 3\rho_i c_i/R_{axis}$.

It should be noted that the pitch is not the local pitch value, but rather the maximum pitch along the orbit, i.e. the pitch value at the outer midplane, ξ_{max}, characterizing the orbit topology. Its value can be roughly estimated from the local ξ value as

$$\xi_{max} \approx \sqrt{1-\frac{R}{R_{axis}+\rho a_{plas}}\left(1-\xi^2\right)},$$

where a_{plas} is the plasma minor radius, R_{axis} is the major radius at the magnetic axis and R is the local major radius.

Figure 2 displays the radial profiles of D_E and D_B for both a 3.5 MeV alpha and a 1 MeV NBI deuteron. Since the diffusion coefficients are pitch dependent, they are calculated for three extreme orbit topologies: (i) strongly passing (ξ_{max} = 0.95, small Larmor radius) (ii) strongly trapped (ξ_{max} = -0.05, large Larmor radius) and (iii) 'marginally trapped' orbit (ξ_{max} = 0.40, large banana orbit width). The term 'marginally trapped' should be taken with a grain of salt because, for a given particle pitch, the orbit is marginally trapped only in a limited region of the plasma. The anomalous diffusion is clearly more significant for NBI deuterons than for fusion alphas. It is also obvious that while the energy scaling of the anomalous diffusion due to magnetic turbulence is more worrisome, its absolute values generally remain small compared with that due to electrostatic turbulence. Another interesting observation is that the anomalous diffusion is strongest for passing orbits.

4. Simulation results

The simulations are carried out for ITER scenario 2, which is a standard H-mode with TF strength of $B_T = 5.3$ T and plasma current $I_p = 15$ MA. The plasma profiles are shown in figure 3, and the ripple map with and without the effect of ferritic inserts is shown in figure 4. The maximum ripple strength along the separatrix for unmitigated ripple is δ = 1.1%, and is reached slightly above the outer midplane. The ferritic inserts reduce this value down to 0.32%. The effect of TBMs could not be included because an accurate 3D field description for scenario 2 was not available yet. Therefore the focus of this study is to get a first estimate on how strongly the various non-neoclassical transport mechanisms transport fusion alphas from the core to the edge region, where ripple-induced transport can channel them to the wall. The presence of TBMs will naturally change the results, but earlier studies of the additional transport induced by TBMs have indicated that the changes are not as dramatic as was originally feared, and remain within an acceptable range [8].

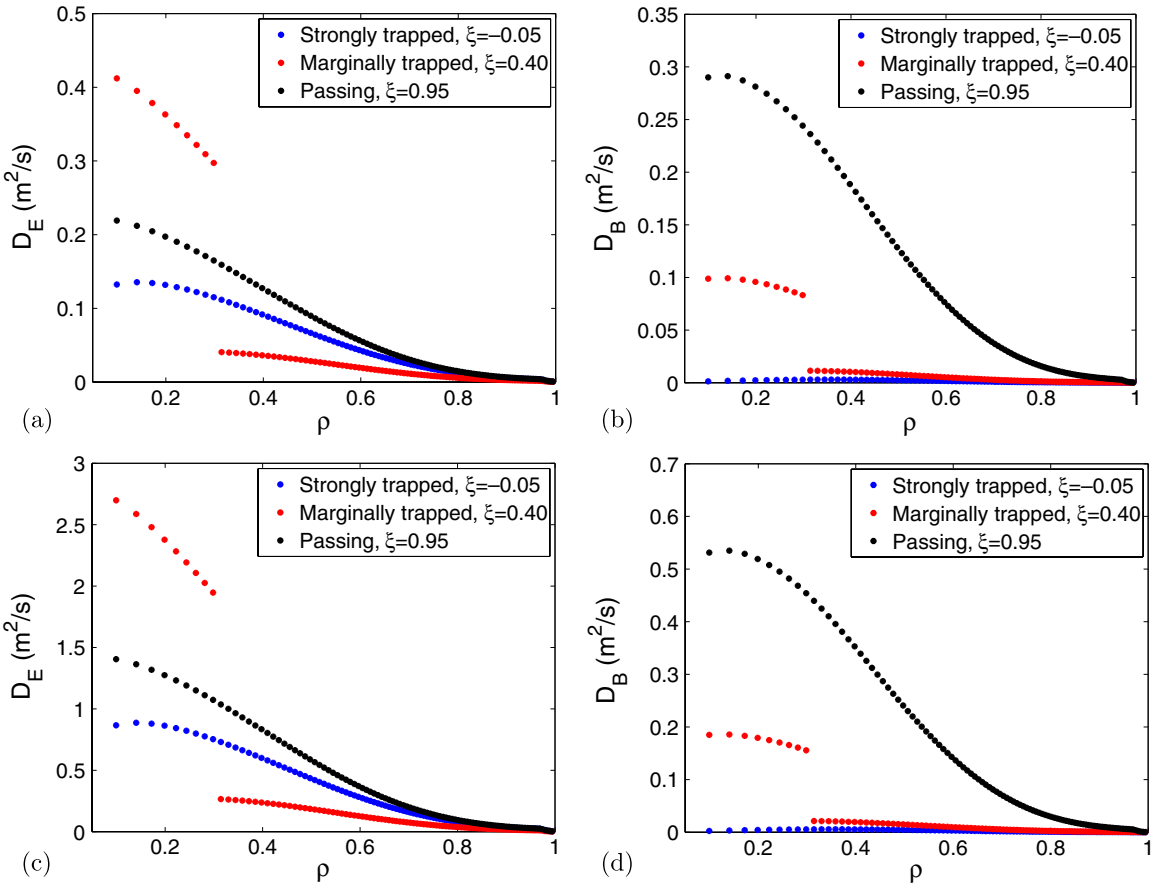

Figure 2. Radial profiles of (*a*) D_E and (*b*) D_B for three extreme alpha particle orbits. Similar plots for a 1.0 MeV deuteron, (*c*) and (*d*), demonstrate the energy dependencies in anomalous transport due to electrostatic and magnetic turbulence. The discontinuity in the diffusion coefficient corresponding to the marginally trapped orbit is due to the change in orbit topology at that radius.

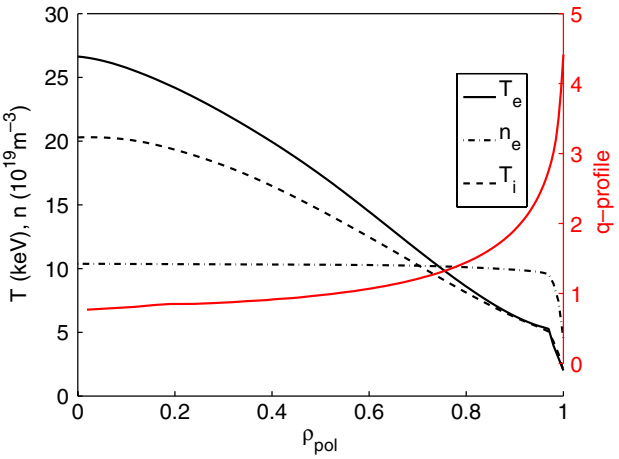

Figure 3. Plasma temperature, density and q-profile in ITER scenario 2.

The simulations are carried out using 50 000 test particles representing alphas born in thermonuclear fusion reactions. Each particle is initialized by choosing its R and z coordinates at random, between maximum and minimum dimensions set by the wall and the plane going through the X-point. If the chosen location is not between $\rho = 0$ and $\rho = 1$, it is discarded and a new location is picked. Once all locations are specified, the particle weight factor is calculated as

$$w_i = \frac{\int_0^{2\pi} r_{\mathrm{F},i}\,\mathrm{d}\phi}{\sum_{i=1}^{N}\int_0^{2\pi} r_{\mathrm{F},i}\,\mathrm{d}\phi}\int_0^1 r_{\mathrm{F}} V\,\mathrm{d}\rho, \qquad (14)$$

where w_i is the weight of the ith particle, $r_{\mathrm{F}}(\rho)$ is the DT fusion reaction rate with $r_{\mathrm{F},i}$ being the rate evaluated at the location of the ith particle, N is the total number of particles and $V(\rho)$ is the flux surface volume.

The test particles are followed until they either intersect a first wall component or are slowed down below 100 keV, or below twice the local thermal energy in the case of NTM simulations, at which point they can be considered as part of the Maxwellian tail of the thermal population. The orbit integration is carried out using a hybrid-method combining GC following and full-orbit tracing. When an ion GC is found to be within a Larmor radius from a wall element, the latest GC time step is cancelled and repeated by following the full Larmor orbit. The ion position is initialized using a random gyro angle. FO simulation is then continued until the ion either hits a wall element or its GC recedes beyond a Larmor radius from the nearest wall element, in which case the GC model is again adopted in order to save CPU time. The switch to the GC position can be made without introducing a spatial error by solving the GC equations of motion along with the FO equations. This method is illustrated in figure 5

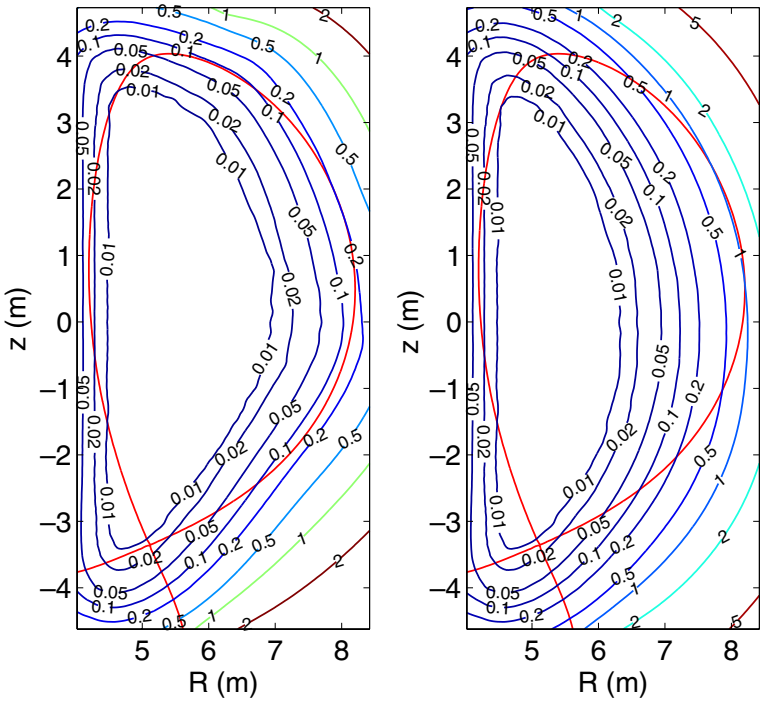

Figure 4. Contours of ripple strength percentage in ITER scenario 2 with (*a*) ferritic inserts and (*b*) no ferritic inserts.

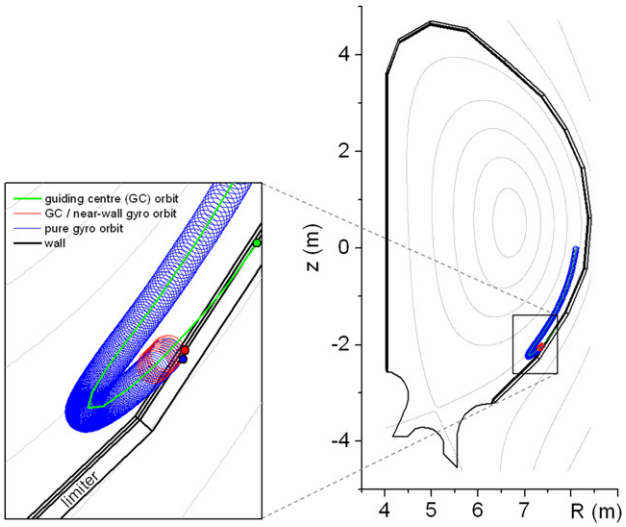

Figure 5. Due to the large Larmor radius of fusion alphas, GC simulations do not give an accurate picture of alpha wall loads. By switching to FO simulation within a Larmor radius of the wall, more accurate load profiles are obtained at minimal CPU cost. In this figure, a GC wall collision is compared with a full gyro-orbit wall collision, and to a hybrid model.

In ASCOT, particle motion can be solved in either Cartesian or Boozer–White coordinates. The physics models described in this paper set requirements on which coordinate systems must be used and, therefore, all results are not produced in the same coordinates. The magnetic island model requires Boozer–White coordinates, while the ripple and FO models require Cartesian coordinates. In addition, on open field lines only Cartesian coordinates can be used. However, the coordinate system may be changed when crossing the separatrix, which allows wall loads to be evaluated even in the case of magnetic islands.

ITER wall design has undergone several revisions due to the strong geometrical constraints imposed on the location of the FIs as well as due to financial constraints. So far two limiter designs have been considered. A design with two limiters in opposite equatorial ports, presented in [27], was used in the simulations reported in [8], where two different FI configurations were considered. However, this design was later abandoned by ITER and a design with poloidal limiters around each port is now favoured. Thus there is a limiter-like structure in every coil period. A simplified model of this new design is given in [17] and has been included in ASCOT. The model is periodic in 20° sectors, and the limiters, each 10° wide at the base, protrude 8 mm from the port face at the equatorial plane. The limiters cover the whole poloidal cross section, except for the divertor region, which is assumed axisymmetric. A panoramic picture of both wall designs is given in figure 6, together with the power loads given by ASCOT simulations. In all simulations to be presented in this paper, the most recent ITER wall with 18 limiters ('continuous limiter design') is used.

4.1. Turbulent transport

Using the turbulent transport coefficients introduced in section 3, we have studied their influence on the fast ion population and, in particular, on the wall power fluxes. We have carried out three different simulations in order to distinguish different mechanisms: (i) with an axisymmetric magnetic background, to see the effect of just the turbulent transport. This is carried out with the latest ITER limiter design; (ii) with a 3D magnetic background including the uncompensated ripple to capture possible synergies between

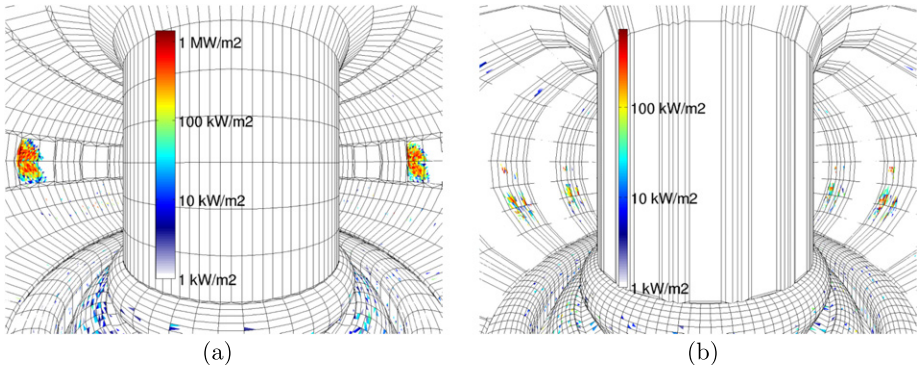

Figure 6. A panoramic picture of the ITER limiter design with (*a*) two and (*b*) 18 limiters. The power load due to thermonuclear alphas in scenario 2, as simulated by ASCOT, is also shown indicating the superiority of the new 18-limiter configuration as far as fast particle loads are concerned.

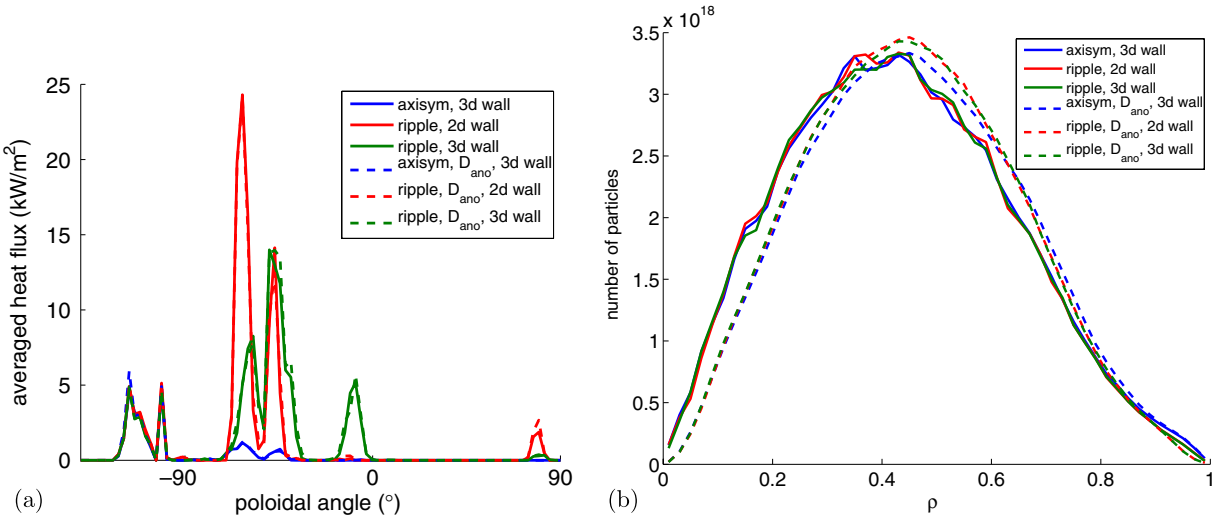

Figure 7. Results of simulations using the turbulent diffusion model. Solid lines represent cases without turbulent diffusion and dashed lines cases with turbulent diffusion. Three different geometries have been considered. Blue: an axisymmetric magnetic field with a 3D wall including 18 limiters. Red: a 3D magnetic background with ripple and an axisymmetric wall. Green: a 3D magnetic background with ripple and a 3D wall with limiters. Figure (*a*) shows the toroidally averaged wall loads and (*b*) the steady-state distribution of the total number of fast ions. The outer midplane corresponds to $\theta = 0^\circ$, and the outer divertor region is at around $\theta = 100^\circ$. The radial coordinate ρ corresponds to the alphas poloidal flux, recall section 3.

ripple-enhanced and turbulent diffusion. This simulation was carried out with both an axisymmetric wall; and (iii) the latest ITER limiter design. For comparison, all of these simulations were also repeated in the absence of turbulent diffusion.

Figure 7 shows both the toroidally averaged heat flux on the PFCs, figure 7(*a*), and the radial distribution of fast ions, figure 7(*b*), from these simulations. The solid lines stand for simulations where only neoclassical diffusion was active, while the dashed lines correspond to simulations where turbulent diffusion, as described by the coefficients displayed in figure 2, was turned on.

Figure 7(*b*) displays the *number* (not density) of fusion alphas in radial slots of fixed size in ρ-space. It should be kept in mind that this distribution is not monoenergetic but represents the slowing-down distribution of the 3.5 MeV alphas. All distributions with turbulent diffusion are found to be shifted outwards. The effect of ripple can be seen as a depletion of the distribution in the edge region, outside $\rho_{\mathrm{pol}} = 0.9$. Qualitatively, the turbulent diffusion thus redistributes the core fast ions, but quantitatively the changes are quite small, particularly in the edge. As a consequence, the wall loads presented in figure 7(*a*) show no reaction to the turbulent diffusion, but are defined by the geometry of the magnetic field and the wall: in the absence of ripple, most heat load is found in the divertor region. Introducing the ripple causes the largest heat flux to be deposited on the bottom part of the main wall, where the plasma is closest to the PFCs. When the full 3D structure of the wall is taken into account, another heat deposition region is found slightly below the midplane.

It should be noted that recent gyrokinetic studies of the effect of turbulence on fast ions [28] have yielded even smaller diffusion coefficients. Therefore, at least based on the present model, it appears very unlikely that turbulent transport of fast ions is going to be a major threat for the ITER wall components.

4.2. NTM-type islands

As described in section 2, at present the numerical model for magnetic islands in ASCOT operates in Boozer–White coordinates that are implemented only for axisymmetric

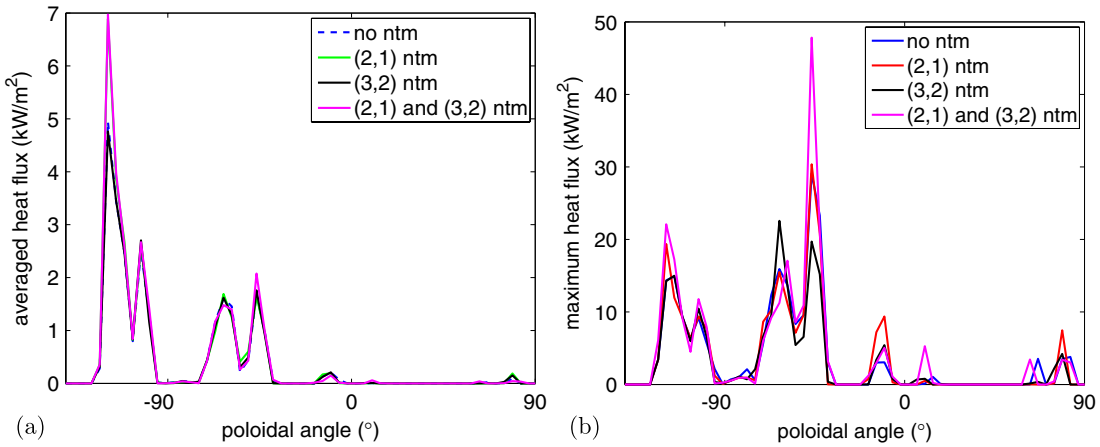

Figure 8. (*a*) Toroidally averaged heat flux on the most recent ITER wall design for the axisymmetric ITER scenario 2 with and without NTM's and (*b*) toroidal maximum of the heat flux for the same cases.

situations. However, an alternative approach to modelling magnetic islands by incorporating them in the background field is currently under development, and the total effect of islands, turbulent transport and 3D field aberrations will be reported once this model is implemented and tested. As the anomalous diffusion was not found to redistribute fast particles dramatically, the NTM simulations will be carried out also without anomalous diffusion.

Figure 8(*a*) shows the toroidally averaged wall load due to fusion alphas in scenario 2 for four different cases: pure neoclassical transport (blue), with only a (2,1) island added (red), with only a (3,2) island added (black), and including both a (2,1) and a (3,2) island (magenta). All NTMs are found to increase the peak power load, and the effect is strongest for the (2,1) mode that is closer to the plasma edge than the (3,2) mode. By including both modes in the plasma, the wall load is not increased from the (2,1)-only case, which is a sign of uncoupled modes. The overall increase in the power load is about a factor of two. Figure 8(*b*) displays the maximum heat flux on the wall from the same simulation. Comparison of figures 8(*a*) and (*b*) shows how misleading the averages can be, not only quantitatively but, more importantly, in giving the poloidal location of maximal heat flux on the wall. The heat flux maxima are in reality found on the limiters, while the toroidally averaged values would put the peak heat fluxes at the divertor. The reason for this is the space between the limiters, with practically zero heat flux, that will dominate the toroidal average in the main chamber. The maximum heat flux for both (2,1) and (3,2) islands is roughly 50 kW m^{-2}, which is 20 kW m^{-2} more than the case without NTMs. Interestingly, the presence of an (3,2) NTM seems to decrease the maximum at the limiter region. The reason for this is probably redistribution of the island, assumed stationary in this study. It is, however, very difficult to deduce from these results how the magnetic ripple and NTMs will interplay.

We have also studied the effect of the mode amplitude on the fast ion losses by scanning the amplitude, i.e. the island width. Figure 9 shows the island width as a function of the square root of the mode amplitude $A_{m,n}$. The points are found to lie roughly on a line, as theory predicts [29]. These six different islands widths were used to calculate the wall load caused by the (2,1) and (3,2) NTMs, and the results are

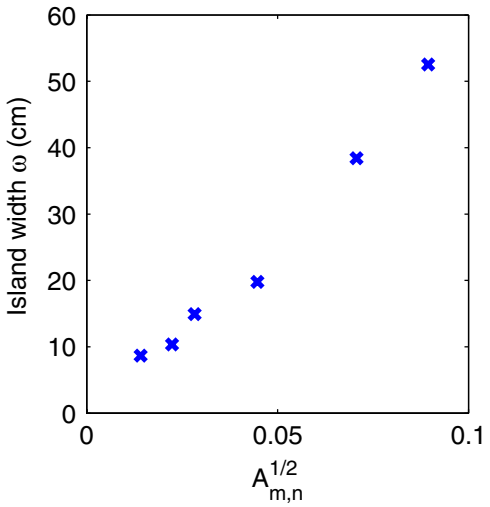

Figure 9. Island width as a function of the square root of the perturbation amplitude.

shown in figure 10. The peak load for the two extreme cases (with up to 50 cm wide islands, clearly unrealistic assuming a successful operation of ITER) becomes comparable to the ripple cases shown in figure 7 (red and green lines). This is due to the fact that, for such strong amplitudes, the island structures overlap and a stochastic region between the islands is formed. Nonetheless the peak load still remains below the engineering limit (∼0.1 MW m^{-2} for the first wall components [1]). The situation might, however, change dramatically when the magnetic field ripple is combined with the NTM islands. Then these two periodic perturbations could interact and form a stochastic region even with smaller perturbation amplitudes.

5. Conclusions and future work

In our continuing effort to obtain ever more quantitatively reliable estimates for fast ion power loads on ITER first wall, we have upgraded the Monte Carlo orbit-following code ASCOT so that, in addition to accommodating 3D magnetic structures and first wall geometries, it is now equipped with numerical models for turbulent transport and NTM-type

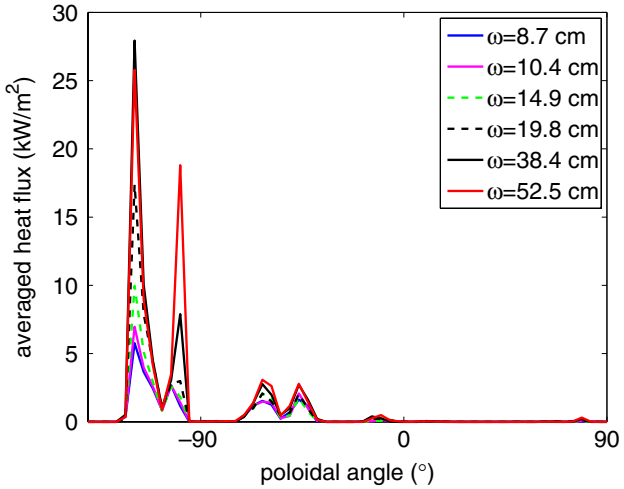

Figure 10. Toroidally averaged heat fluxes obtained from a scan of island widths.

islands, and it also allows the GC formalism and gyro-orbit following to be chosen between.

The simulations utilizing these new features were carried out for ITER scenario 2, which will be the workhorse of ITER, and for the most recent wall configuration, the 'continuous limiter' design. The simulation results indicate that when ripple is not taken into account, most of the power load is found at the divertors and is very low. In the case of turbulent diffusion, even using turbulence parameters that are found to be excessive compared with recent gyrokinetic turbulence simulations, the wall loads with and without this kind of anomalous transport are identical. Turbulent transport is, however, found to affect the fast ion distribution further inside the plasma, but even there the effect is small. Including the NTM-type islands is found to cause an overall increase in the heat flux to the first wall but, somewhat surprisingly, not to affect the structure of the distribution on the wall.

Including the ripple, however, produces peak power loads on the first wall that can be ten times higher than at the divertors. The peak is not located at the outer midplane, as it was in the earlier limiter design with only two, poloidally localized limiters at around the midplane on opposite sides of the torus. These limiters were found to receive practically all the fast ion power. With both a 2D wall model and the new, semi-continuous and poloidally extended limiter design, the majority of the power is now found on the limiter structures well below the midplane, in the region where the plasma is closest to the wall. The realistic 3D wall exhibits yet another power peak right below the midplane that is absent in the 2D wall simulations. Including turbulent transport does not bring any changes in the wall distribution even with the excessive turbulence parameters used in the simulations. Therefore, at least with the present theory-based model for turbulent transport, microturbulence does not seem to pose a serious threat for the integrity of the vessel wall as far as fast ions are concerned.

We also addressed the issue of 3D wall geometry in ITER by comparing the power loads obtained for the earlier wall design with two limiters localized in the region of the outer midplane and the current design with 18 poloidally extended limiters. The latter, semi-continuous limiter was found to be more beneficial as far as the fast ion loading of the first wall is concerned.

The most important shortcomings of this work are the following: (i) the NTM study was carried out only for the axisymmetric case because this assumption is built into the numerical model currently implemented in ASCOT. (ii) All cases were simulated without the presence of TBMs because a magnetic background where the effect of TBMs is taken into account with sufficient accuracy was not yet available for scenario 2. We are currently working on an alternative method of incorporating the magnetic islands even in a non-axisymmetric situation, thus permitting studies that simultaneously include the effect of toroidal ripple, TBMs and the field perturbation produced by resonant magnetic perturbation (RMP) coils that are envisaged to be used for ELM mitigation. On the other hand, the islands modelled in this work were fairly deep in the plasma, and it is expected that when ripple is included, their effect on wall power loads will not be significant.

We shall also repeat this study for NBI-generated ions. The properties (energy and pitch dependencies) of the turbulent diffusion model suggest that the NBI-generated ions are probably more vulnerable to this transport mechanism than the higher-energy fusion alphas born with isotropic velocity distribution. Furthermore, at least at higher densities, also the (2,1) NTMs could have a bigger impact on NBI-ions than on fusion alphas. Finally, all the analyses will be repeated for scenario 4. For scenario 4, the situation regarding particle species is quite different due to the lower plasma current, and the earlier, purely neoclassical study found the NBI-injected ions to be just as detrimental to the wall structures as the fusion alphas.

Acknowledgments

This work was partially supported by the Academy of Finland Projects Nos 121371 and 134924, and the European Communities under the contract of Association between EURATOM/TEKES. The simulations were performed using the computational facilities of CSC, the Finnish IT Center for Science.

References

[1] Fasoli A. *et al* 2007 Chapter 5: Physics of energetic ions *Nucl. Fusion* **47** S264

[2] Goldston R.J., White R.B. and Boozer A.H. 1981 Confinement of high-energy trapped particles in tokamaks *Phys. Rev. Lett.* **47** 647–9

[3] Mimata H., Tani K., Tobita K., Tsutsui H., Tsuji-Iio S. and Shimada R. 2006 Finite larmor radius effects on ripple diffusion in tokamaks *Prog. Nucl. Energy* **50** 638–42 Innovative nuclear energy systems for sustainable development of the world. *Proc. 2nd COE-INES Int. Symp. INES-2 (Yokohama, Japan, 26–30 November 2006)*

[4] Shinohara K., Oikawa T., Urano H., Oyama N., Lonnroth J., Saibene G., Parail V. and Kamada Y. 2009 Effects of ferromagnetic components on energetic ion confinement in ITER *Fusion Eng. Des.* **84** 24–32

[5] Chuyanov V.A., Campbell D.J. and Giancarli L.M. 2010 TBM program implementation in ITER *Fusion Eng. Des.* **85** 2005–2011

[6] Salavy J.-F., Boccaccini L.V., Chaudhuri P., Cho S., Enoeda M., Giancarli L.M., Kurtz R.J., Luo T.Y., Bhanu Sankara Rao K. and Wong C.P.C. 2010 Must we use ferritic steel in TBM? *Fusion Eng. Des.* **85** 1896–902
[7] Giancarli L. *et al* 2010 Preparation of interfaces in ITER for integrating the test blanket systems *Fusion Eng. Des.* **85** 1829–33
[8] Kurki-Suonio T. *et al* 2009 ASCOT simulations of fast ion power loads to the plasma-facing components in ITER *Nucl. Fusion* **49** 095001
[9] Günter S. *et al* 2007 Interaction of energetic particles with large and small scale instabilities *Nucl. Fusion* **47** 920
[10] Hauff T., Pueschel M.J., Dannert T. and Jenko F. 2009 Electrostatic and magnetic transport of energetic ions in turbulent plasmas *Phys. Rev. Lett.* **102** 075004
[11] Vlad G., Briguglio S., Fogaccia G., Zonca F. and Schneider M. 2006 Alfvènic instabilities driven by fusion generated alpha particles in ITER scenarios *Nucl. Fusion* **46** 1
[12] Buttery R.J. *et al* 2000 Neoclassical tearing modes *Plasma Phys. Control. Fusion* **42** B61
[13] Heidbrink W.W. and Sadler G.J. 1994 The behaviour of fast ions in tokamak experiments *Nucl. Fusion* **34** 535
[14] Pinches S.D. *et al* 1998 The hagis self-consistent nonlinear wave-particle interaction model *Comput. Phys. Commun.* **111** 133–49
[15] White R.B. and Chance M.S. 1984 Hamiltonian guiding center drift orbit calculation for plasmas of arbitrary cross section *Phys. Fluids* **27** 2455–67
[16] Snicker A., Kurki-Suonio T. and Sipilä S.K. 2010 Realistic simulations of fast-ion wall distribution including effects due to finite larmor radius *IEEE Trans. Plasma Sci.* **38** 2177–84
[17] Putvinski S. 2010 *ITER Report* UID:2MSCAL. https://user.iter.org/?uid=2MSCAL&action=get_document
[18] Strumberger E., Günter S., Merkel P., Schwarz E. and Tichmann C. 2010 Self-consistent three-dimensional computations of non-axisymmetric iter equilibria *Nucl. Fusion* **50** 025008
[19] Strumberger E., Günter S., Schwarz E., Tichmann C. and The ASDEX Upgrade Team 2008 Fast particle losses due to NTMS and magnetic field ripple *New J. Phys.* **10** 023017
[20] White R.B. and Boozer A.H. 1995 Rapid guiding center calculations *Phys. Plasmas* **2** 2915–9
[21] Igochine V., Dumbrajs O., Constantinescu D., Zohm H., Zvejnieks G. and The ASDEX Upgrade Team 2006 Stochastization as a possible cause for fast reconnection during mhd mode activity in the asdex upgrade tokamak *Nucl. Fusion* **46** 741
[22] Snicker A., Poli E. and Kurki-Suonio T. 2010 Neoclassical tearing modes in ASCOT code *European Physical Society 37th Conf. on Plasma Physics (Dublin, Ireland, 2010)* http://ocs.ciemat.es/EPS2010PAP/pdf/P5.187.pdf
[23] La Haye R.J., Isayama A. and Maraschek M. 2009 Prospects for stabilization of neoclassical tearing modes by electron cyclotron current drive in ITER *Nucl. Fusion* **49** 045005
[24] Boozer A.H. and Kuo-Petravic G. 1981 Monte carlo evaluation of transport coefficients *Phys. Fluids* **24** 851–9
[25] Thilo H. 2009 Transport of energetic particles in turbulent plasmas *PhD Thesis* University of Ulm
[26] Rhodes T.L., Leboeuf J.-N., Sydora R.D., Groebner R.J., Doyle E.J., McKee G.R., Peebles W.A., Rettig C.L., Zeng L. and Wang G. 2002 Comparison of turbulence measurements from DIII-D low-mode and high-performance plasmas to turbulence simulations and models *Phys. Plasmas* **9** 2141–8
[27] Federici G. *et al* 2007 Simulations of ITER start-up and assessment of limiter power loads *J. Nucl. Mater.* **363-365** 346–52 (Plasma-Surface Interactions-17)
[28] Albergante M., Graves J.P., Fasoli A., Jucker M., Lapillonne X. and Cooper W.A. 2011 Numerical modelling of electromagnetic turbulent transport of energetic ions in burning plasmas *Plasma Phys. Control. Fusion* **53** 054002
[29] Waelbroeck F.L. 2009 Theory and observations of magnetic islands *Nucl. Fusion* **49** 104025